Amorphous Features of Working Catalysts: XAFS and XPS Characterization of Mn/Na$_2$WO$_4$/SiO$_2$ as Used for the Oxidative Coupling of Methane

Yuan Kou,[*,1,2] Bing Zhang,[*] Jian-zhong Niu,[*] Shu-ben Li,[*] Hong-li Wang,[†]
Tsunehiro Tanaka,[‡] and Satohiro Yoshida[‡]

[*]*State Key Laboratory for Oxo Synthesis and Selective Oxidation, Lanzhou Institute of Chemical Physics, Chinese Academy of Sciences,
Lanzhou 730000, China;* [†]*State Key Laboratory of Catalysis, Dalian Institute of Chemical Physics, Chinese Academy of Sciences,
Dalian 116023, China; and* [‡]*Department of Molecular Engineering, Kyoto University, Kyoto 606-01, Japan*

Mn/Na$_2$WO$_4$/SiO$_2$ catalyst for the oxidative coupling of methane has been investigated by using the *L*-edge and the *K*-edge XAFS and XPS. The surface of the fresh catalyst is found to be dominated by oxygen-enriched amorphous phases consisting of discretely distributed tetrahedral WO$_4$ and octahedral MnO$_6$ groups. The average bond lengths, which is 1.77 Å for W–O and 2.00 Å for Mn–O, are fully identical to those in pure Na$_2$WO$_4$ and Mn$_2$O$_3$. However, on the used catalyst after a 450 h run, almost no tungsten species is detectable. Instead, tetrahedral manganese sites are observed. The surface of the used catalyst is dominated by highly dispersed MnO$_4$ groups consisting of tetrahedral and coordinatively unsaturated octahedral sites. The average Mn–O bond length increases to 2.09 Å while the Mn 2p$_{3/2}$ binding energy increases from 641.4 eV (Mn^{3+}) to 641.7 eV (Mn^{2+}). These results suggest that the combination of tetrahedral and octahedral metallic cores with different oxidation states from each other is responsible for the catalysis in the oxidative coupling of methane, and that the high activity of the manganese-tungsten catalyst is due to the surface oxygen species, which are pre-activated from lattice oxygens to "the nearest oxygens" by the surface in an amorphous state. © 1998 Academic Press

I. INTRODUCTION

Silica-supported manganese-tungsten catalyst, Mn/Na$_2$WO$_4$/SiO$_2$ has received increased attention as a catalyst for the oxidative coupling of methane because of its excellent catalytic performance (1–9). A C$_{2+}$ selectivity of 65% at 37% methane conversion was firstly reported by Li and his co-workers. Further studies using either XRD, XPS and PASCA (positron annihilation spectroscopy for chemical analysis) (3), or Raman and EPR (4) proposed that W–O–Si species were responsible for the oxidative coupling of methane via a redox mechanism. Recently, a

C$_{2+}$ selectivity in excess of 80% at a CH$_4$ conversion of 20% over this catalyst was repeatedly confirmed by Lunsford group. By comparison with the catalytic behaviors over Mn/Na$_2$WO$_4$/MgO and NaMnO$_4$/MgO catalysts, the authors suggested that Na–O–Mn species were the most possible active sites (8). However, studies on Na$_2$WO$_4$/CeO$_2$ by the same group, which gave a C$_2$ selectivity of 70% at a CH$_4$ conversion of 22%, seemed to be at variance with this suggestion (7).

Activation of lattice oxygen in the oxidative coupling of methane has been extensively studied (10–16). Bulk lattice oxygen ions (O^{2-}) do not participate directly in the reaction since the existence of the active sites is sustained only in the presence of gas-phase O$_2$ (7). Transport of gas-phase oxygen molecules to lattice oxygen ions over surface catalytic sites is the key step toward the formation of active oxygen species, and is therefore of intense interest.

Recently, a 450 h stability test for the Mn/Na$_2$WO$_4$/SiO$_2$ catalyst has been carried out in a 200 ml fluidized bed reactor under the conditions: 800–875°C, CH$_4$: O$_2$: H$_2$O = 6 : 1 : 3, and GHSV$_{CH_4}$ = 7000 h^{-1} (9). A consistent C$_2$ yield of 17.8–19.4% with a C$_{2+}$ selectivity of 82.6–75.7% has been obtained without exception even for the last day. The fresh catalyst and the catalysts after a 100 h, and a 450 h run, respectively, were collected. In this paper, the geometric and electronic structure of the three samples are studied and compared with one another by using W $L_{I,III}$-edge and Mn *K*-edge XAFS (X-ray Absorption Fine Structure) and XPS. The amorphous feature of the catalyst surface is recognized and a combination of tetrahedral tungsten sites and octahedral manganese sites is proposed to be essential for the formation of an active ensemble on the catalyst service.

II. EXPERIMENTAL

Three practical catalyst samples are studied. The catalyst as prepared, the catalyst took out from the fluidized bed

reactor after 100 h run, and the catalyst discharged from the reactor after 450 h run are named as fresh catalyst, 100 h catalyst, and 450 h catalyst, respectively, in this paper. Both the used catalysts were obtained without protection from air since the samples were known to be very stable in air. For instance, for the samples studied here, no further oxidation from Mn^{2+} to Mn^{3+} was observed even after one month. All the samples as received were therefore simply kept in a dryer before making the analyses.

XPS analysis of the catalysts was performed with VG ESCALAB 210 spectrometer, in which the samples in the form of pressed wafers could be heated *in situ* under UHV to 620°C. A Mg or Al target as the anode of X-ray source with a power of 300 W was used. The pass energy of the analyzer was 25 eV in a step increment of 0.05 eV. The dwell time employed was 60 ms. The binding energy of all spectra was calibrated with respect to the Si 2p line at 103.4 eV.

Infrared measurement was recorded on a Fourier transform, high resolution IFS 120 (Bruker) spectrometer using pressed disk for all the samples.

X-ray absorption data were obtained at the Photon Factory (Tsukuba, Japan) on beamline BL-7C. A Si(111) double-crystal monochromator with a positron beam energy of 2.5 GeV and an average stored current of 250 mA was employed. Data for reference compounds were collected in transmission mode while those for supported catalysts were collected in fluorescence mode. Specimens were made by directly applying the fine powders to Scotch tape. The measurements were carried out at room temperature.

The energy scale of the W L-edge and the Mn K-edge XANES (X-ray Absorption Near Edge Structure) spectra (both in 0.5 eV steps) was calibrated relative to Na_2WO_4, and MnO_2, respectively, using the first derivative of the spectrum. The XANES spectra were normalized by fitting a cubic spline μ_0 to the EXAFS (Extended XAFS) region of the data, and by fitting a linear function to the pre-edge data. The spectra were then further normalized to unit step height. The EXAFS oscillation was determined by $\chi(k) = (\mu - \mu_0)/\mu_0$. The $k^n\chi(k)$ ($n = 2$ for the W edge and $n = 3$ for the Mn edge) was Fourier transformed into r-space by a Hanning window function in the range $k = 1.5$ to 14.0 for the L_{III}-edge and $k = 1.5$ to 12.0 for the K-edge. The Fourier transform containing the peaks of interest was filtered into k-space by a Hanning window function. A least-squares curve-fitting was then performed to calculate the structural parameters for each shell using the theoretical components determined by FEFF3.25 code (17). The reduction factor used, S_0^2, was 0.75, which was determined by the best fits to the filtered-EXAFS of the nearest coordination shell of the reference compounds. The parameter error estimates were calculated by the recommended method (18). The correlations between the variables were estimated by the standard method (19).

III. RESULTS AND DISCUSSION

1. Amorphous Feature

Figure 1 shows the tungsten L_I-edge XANES of the fresh catalyst $Mn/Na_2WO_4/SiO_2$ and the reference compound Na_2WO_4. The pre-edge feature at the tungsten L_I-edge arises from 2s-5d transitions, which is dipole forbidden for regular octahedral site-symmetry, partly allowed for a distorted octahedral environment, and dipole allowed in the absence of a center of inversion symmetry (20). WO_4 group in Na_2WO_4 has regular tetrahedral symmetry, a fairly intense pre-edge peak as expected is observed. It can be seen from Fig. 1 that the XANES features of the fresh catalyst is virtually identical to those of Na_2WO_4, indicating a tetrahedrally coordinated environment for the supported tungsten cores.

Tungsten L_{III}-edge EXAFS-derived Fourier transforms of Na_2WO_4 and the fresh catalyst are shown in Fig. 2. Crystalline metal oxides generally show very intense metal-metal contribution in the range of 2.5 to 3.5 Å in their Fourier transforms due to the periodically appeared lattices. The feature of crystalline Mn_2O_3 as a good example will be discussed below. Tungstates having the general formula M_2WO_4 (M = alkali metals), however, only contain the discrete tetrahedral ions WO_4^{2-} (21). Following the intense W–O shell centered at 1.4 Å (not corrected for phase shift), it can be seen from Fig. 2 that Na_2WO_4 merely shows a very weak nearest tungsten contribution at 2.5 Å due to lack of long-range-order. However, even this very weak contribution from the nearest tungsten has also disappeared in the spectrum of the fresh catalyst while the W–O shell shows no change, revealing an amorphous characteristic
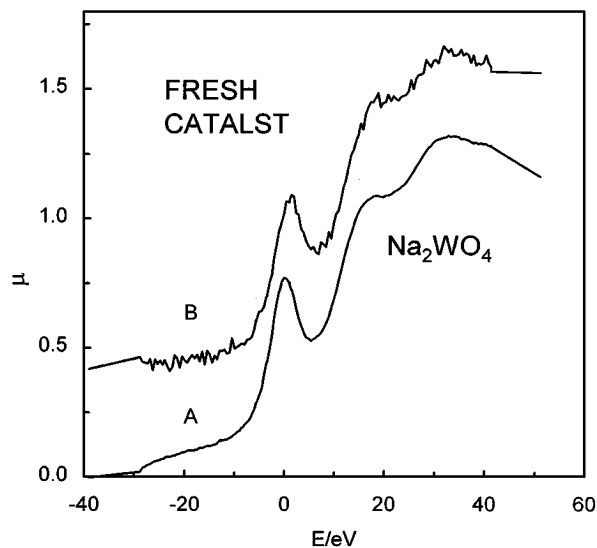

FIG. 1. The tungsten L_I-edge XANES spectra for the fresh catalyst and the reference compound Na_2WO_4.
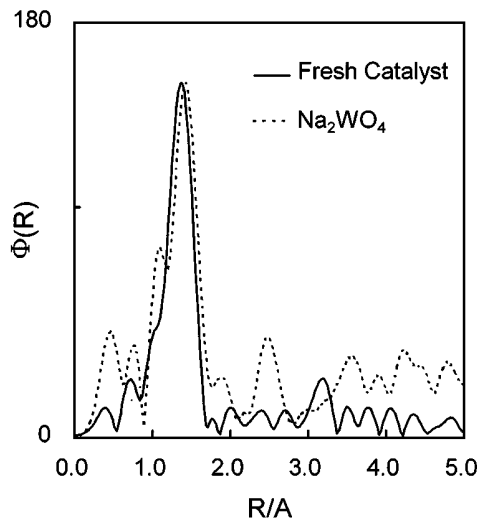
FIG. 2. The tungsten L_{III}-edge EXAFS-derived Fourier transforms for the fresh catalyst and the reference compound Na_2WO_4 (dashed line).

for the supported tungsten species. Further amplitude analysis and testing fits to the EXAFS oscillations filtered from the weak peaks above 2.5 Å in the transform of the fresh catalyst (solid line in Fig. 2) suggest that these peaks probably contain contributions from at least two different neighbors, that is, 1–2 manganese atom(s) at about 3.5 Å and 2–3 tungsten atoms at about 3.4 Å. It can be seen from Fig. 3 that testing fit to the peaks in the range of 2.8–3.2 Å (solid line in Fig. 2, the peaks included were filtered to k-space and then fitted by FEFF-derived components) by single Mn shell gives the maximum of the envelop at $k = 7.4$ Å^{-1} (Fig. 3A, solid line) while the maximum of the EXAFS-derived curve is at $k = 9.4$ Å^{-1}, implying that some heavier elements are probably involved. Test fit to the same oscillation by single W shell (Fig. 3B) is however unsuccessful. By slightly expending the filtered range to 2.8–3.6 Å, testing fit by a mixture of manganese-tungsten neighbors (Fig. 3C) finally recover all the spectral features especially for the maxima of the envelop.

Mn K-edge EXAFS-derived Fourier transforms of crystalline reference compound Mn_2O_3 and the fresh catalyst $Mn/Na_2WO_4/SiO_2$ are compared in Fig. 4. Following an intense M–O shell, a more intense peak is observed at 2.7 Å in the transform of the Mn_2O_3. This peak arising from the nearest manganese neighbors and the second nearest oxygen reflects the periodic feature of the lattices. It can be found from the transform of the catalyst that the peak at 2.7 Å is significantly diminished. In comparison with the peak area of Mn_2O_3, only about 2/5 is left for the fresh $Mn/Na_2WO_4/SiO_2$, indicating that most of the supported manganese units (about 3/5) lost its long-range-ordered character to form an amorphous phase on the surface. Interestingly, in comparison with that of Mn_2O_3, the Mn–O shell exhibits no change. This situation is very similar to the case

observed for W–O shell when changed from the bulk to the surface, demonstrating that the WO_4 and MnO_6 groups in fact show no structural difference from the pure reference compounds. It means that the discrete distributions of the groups will play a key role for the catalysis.

2. Oxygen-Enriched Surface

The binding energy and near-surface compositions of the catalysts observed by XPS are summarized in Tables 1 and 2,
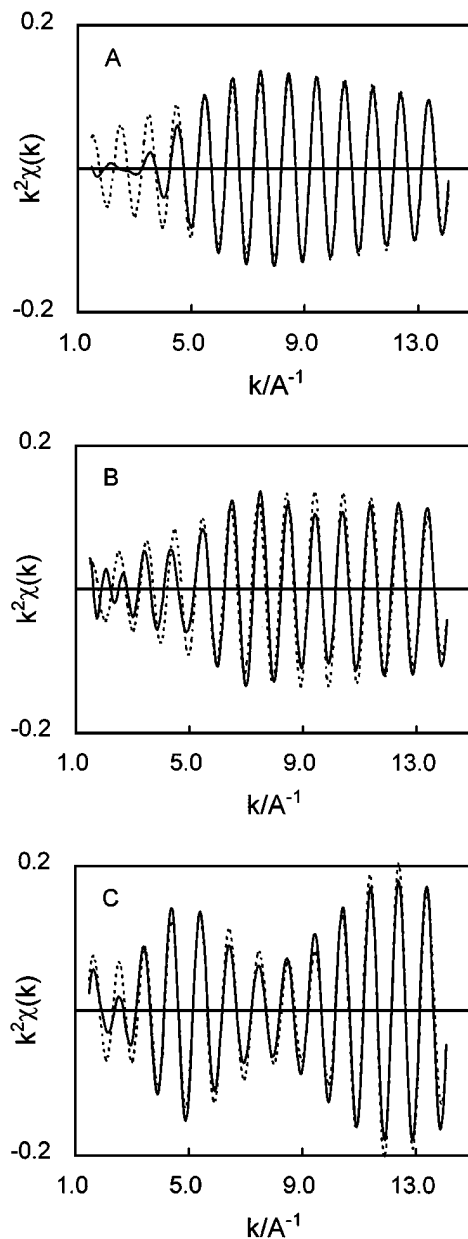

FIG. 3. Testing fit (solid lines) to the EXAFS oscillation filtered from the Fourier transform shown in Fig. 2 in the range (not corrected for phase shilt): (A) 2.87–3.23 Å using single Mn shell; (B) 2.87–3.23 Å using single W shell; and (C) 2.87–3.56 Å using Mn and W shells.
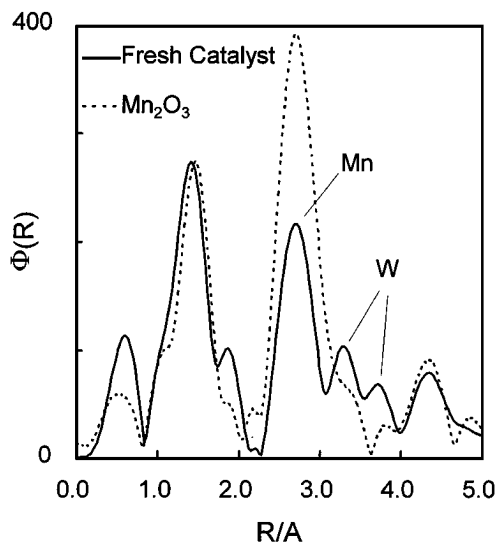
FIG. 4. The manganese K-edge EXAFS-derived Fourier transforms for the fresh catalyst and the reference compound Mn_2O_3 (dashed line).

respectively. Similar results for the fresh catalyst have been recently reported, but the peak at 290 ± 1 eV in the C 1s region was attributed to $CO_3^=$ (8). XPS spectra for the fresh catalyst $Mn/Na_2WO_4/SiO_2$ in the C 1s region by using Mg, and Al anode, respectively, are compared in Fig. 5. The peak at 290 eV is absent altogether by changing the anode from Mg to Al, indicating that the peak is originated from the Na Auger contribution but not $CO_3^=$. A $CO_3^=$ surface species, which produces a C 1s peak at 288.2 eV, has been observed over a 2% Mn/MgO sample (8).

XPS spectra in the Mn 2p region of the fresh catalyst and the same sample "*in situ*" heated to 620°C are shown in Fig. 6. The Mn $2p_{3/2}$ binding energy of 641.4 eV is observed for the fresh catalyst, indicating a predominantly Mn^{3+} phase on the surface. The XANES and EXAFS-derived parameters described below indicate that these Mn^{3+} ions are in the form of Mn_2O_3. By heating to 620°C, a shoulder centered at 646.7 eV is added to the feature. The shoulder is attributed to Mn^{2+}. These Mn^{2+} signals are stable and do not disappear when returning to room temperature unless the sample is further exposed to air for 36 h.

TABLE 1

Observed XPS Binding Energies (eV) of Catalyst Components

Catalyst	Mn 2p	Na 1s	W 4f	Si 2p	O 1s SiO$_2$	O 1s MO$_x$	C 1s
Fresh catalyst	641.4	1071.8	35.3	103.4	532.8	530.6	284.9
in situ at 620°C	641.4	1072.2	35.3	103.4	532.8	530.6	285.0
100 h catalyst	641.9	1071.8	35.5	103.4	532.7	530.6	285.1^a
450 h catalyst	641.7	1072.4	35.4	103.4	532.8	530.8	284.9
in situ at 620°C	641.9	1072.5	35.5	103.4	532.7	530.7	284.6

^{a} A C 1s peak at 289.1 eV attributed to the adsorbed CO was observed.

TABLE 2

Near-Surface Compositions (Mol%) of Catalyst Components

Catalyst	Mn 2p	Na 1s	W 4f	Si 2p	O 1s SiO$_2$	O 1s MO$_x$	C 1s
Fresh catalyst	1.8	9.2	3.0	18.1	40.3	18.8	8.8
in situ at 620°C	1.8	10.3	3.6	19.3	40.1	19.4	5.4
100 h catalyst	2.0	13.0	1.9	8.3	30.6	21.3	18.4^a
450 h catalyst	1.3	2.5	0.2	23.5	51.9	10.4	10.1
in situ at 620°C	2.4	4.5	0.2	24.9	50.8	11.5	5.6

^{a} 2.7% C 1s at 289.1 eV was not included.

The near-surface compositions of the fresh catalyst is enriched not only in Na and W (8), but also in oxygen. The observed oxygen composition is 18.8% for the sample investigated at room temperature. The stoichiometrically estimated percentage for these oxygens is 2.7% for 1.8% Mn, 12% for 3.0% W, and 1.6% for 3.2% Na (the other 6% Na is attributed to Na_2WO_4), giving a percentage of only 16.3% in total. Similar situation in fact could be found from the recent literature (8) if correcting the assignment of 290 ± 1 eV to Na contribution. By heating to 620°C, desorption of surface oxygens is expected. In that case, the oxygen composition observed is 19.3%. Among them, 2.7% is for 1.8% Mn, 14.4% for 3.6% W, and 1.5% for 3.1% Na, giving a total percentage of 18.6%, which apparently comes close to the observed value. However, the formation of Mn^{2+} as demonstrated by the shoulder at 646.7 eV has not been
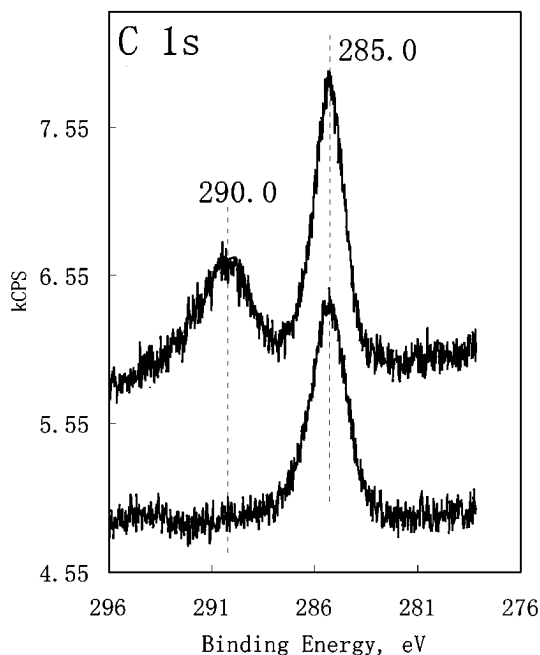

FIG. 5. XPS spectra in the C 1s region of the fresh catalyst by using Mg (upper) or Al (lower) as the anode.
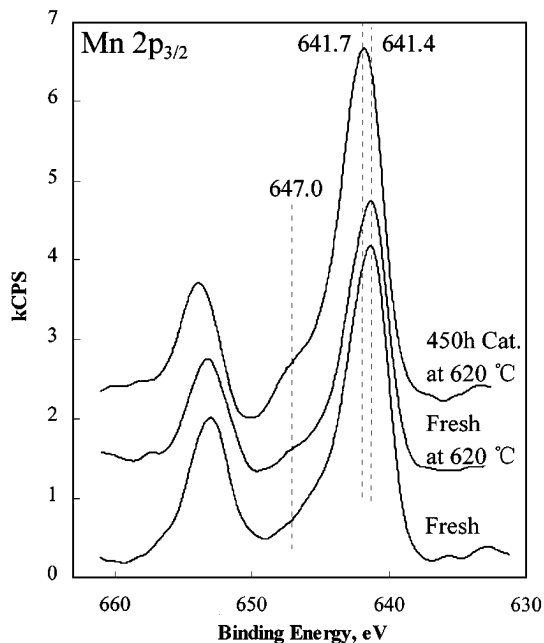
FIG. 6. XPS spectra in the Mn 2p region of (from lower to upper) the fresh catalyst, the fresh catalyst *in situ* heated to 620°C, and the 450 h catalyst at 620°C.

taken into the estimation, confirming that the surface of the catalyst heated to 620°C is still enriched in oxygen. It is the unique feature of the manganese-tungsten catalyst since it is well known that the transport of gas-phase oxygens to lattice oxygens and then to activated oxygen intermediates are the key steps for the oxidative coupling of methane.

3. Detailed Structural Parameters

The amplitude analysis and the testing fits (Fig. 3) to the peaks above 2.5 Å in the W L_{III}-edge EXAFS-derived Fourier transform of the fresh catalyst have shown that the peaks are probably contributed by a mixture of W and Mn neighbors. The best fits listed in Table 3 reveal 4 oxygen neighbors at 1.77 Å, 1.5 tungsten neighbors at 3.38 Å, and 2.1 manganese neighbors at 3.48 Å for the tungsten

core on the fresh catalyst, fully supporting the XANES results that the tungsten is still in a 4-coordinated tetrahedral site. However, two different neighbors like Mn and W having a difference in shell radius less than 1.5 Å in fact are theoretically not possible to be exactly distinguished from each other. Correlation analysis to the parameters is in good agreement with this view. In summary, the best fits indicate that the supported tungsten ions are located into tetrahedral sites on the surface. Within 4 Å, there are some nearest tungsten and manganese neighbors surrounding the sites, but because of the limitation of the EXAFS technique, the fitting parameters for these two shells are not reliable.

The features of the Mn *K*-edge EXAFS-derived Fourier transform of the fresh catalyst shown in Fig. 4 have been briefly discussed. The most intense peak is contributed by the nearest oxygen neighbors. The second intense peak labeled Mn is caused by manganese neighbors while its broad shoulders labeled W are caused by tungsten neighbors. The Fourier-filtered EXAFS oscillations for the peak, and the shoulder, respectively, are compared with one another as shown in Fig. 7. It can be seen from the comparison that the envelop of the EXAFS oscillation filtered from the peak labeled Mn in the transform, Fig. 7B, shows exactly the same feature as that obtained from the manganese contribution in Mn_2O_3 (the strongest peak in the dashed line spectrum shown in Fig. 4), Fig. 7A, but that filtered from the shoulders, Fig. 7C, is completely different. The maximum of the envelop shifts from 6.6 Å^{-1} in Figs. 7A and B to 9.4 Å^{-1} in Fig. 7C, indicating a much heavier metallic neighbor for the central manganese ion.

The best fits summarized in Table 4 and Fig. 8 reveal that, (i) each manganese ion on average has 6 oxygen neighbors at 2.00 Å, indicating a six-coordinated, approximately octahedral site for the manganese center. Similar site-geometry for the supported FeO_6 groups has been described elsewhere (22–24). It appears that the presence of $MnWO_4$ species on the surface (8) is not possible, at least its formation is not significant since each of the manganese ions is

TABLE 3

W L_{III}-Edge EXAFS-Derived Structural Parameters for the W Local Environment in Fresh Catalyst Mn/Na₂WO₄/SiO₂

Shell	R (Å)	CN	DW (Å^{-1})	R-factor
W–O	1.77	4.2	0.0007	0.17
W–W	3.38	1.5	0.0058	
W–Mn	3.48	2.1	0.0033	

Note. Filtered range in *r*-space: 0.7–2.6 Å. Abbreviations: R, shell radius; CN, coordination number; DW, Debye-Waller fact.

TABLE 4

Mn *K*-Edge EXAFS-Derived Structural Parameters for the Mn Local Environment in Fresh and Used Catalysts Mn/Na₂WO₄/SiO₂

Sample	Shell	R (Å)	CN	DW (Å^{-1})	R-factor
Fresh	Mn–O	2.00	6.2	0.0098	0.13
	Mn–Mn	3.14	2.3	0.0058	
	Mn–W	3.57	2.0	0.0055	
	Mn–W	4.22	1.2	0.0143	
Used	Mn–O	2.09	4.3	0.0057	0.13
Mn_2O_3	Mn–O	2.00	6.1	0.0073	0.07
	Mn–Mn	3.13	9.1	0.0101	

Note. Filtered range in *r*-space: 0.7–3.4 Å. Abbreviations: R, shell radius; CN, coordination number; DW, Debye-Waller fact.
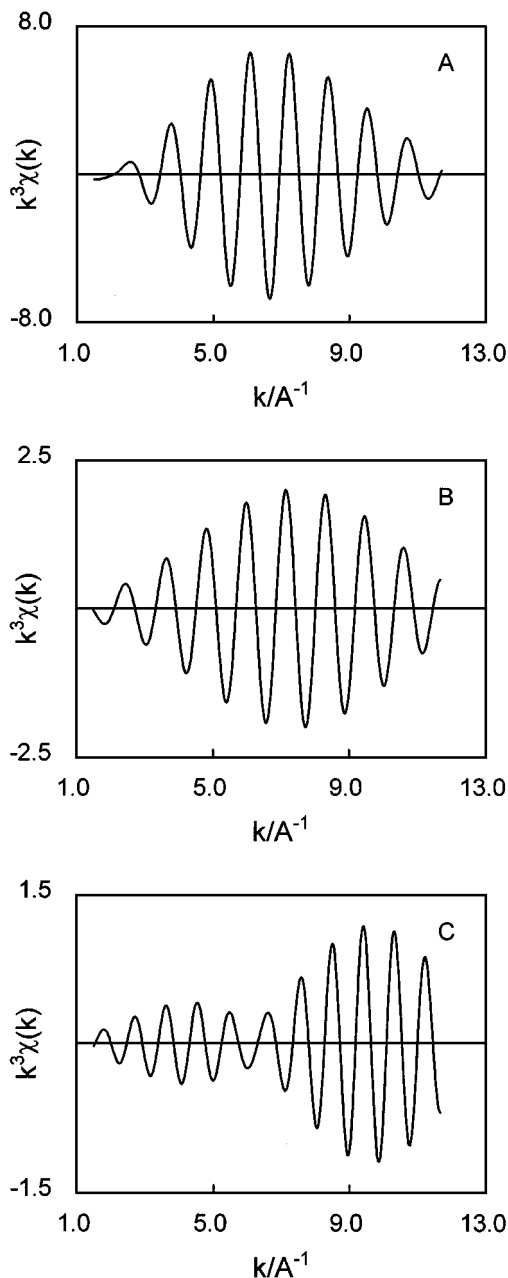
4. About the Used Catalyst

The used catalyst $Mn/Na_2WO_4/SiO_2$ was also investigated by XPS and XAFS techniques. The 100 h catalyst shows no obvious difference from the fresh one based on W $L_{I,III}$-edge and Mn K-edge XAFS analyses. The K-edge XANES spectrum as a part of the 100 h catalyst results has been included in Fig. 11. XPS results of the 100 h catalyst summarized in Tables 1 and 2 indicate that, in comparison with the fresh catalyst, about 1/3 surface tungsten species have disappeared. The Mn 2p binding energy shifts to 641.9 eV while an intense shoulder at 646.7 eV is observed, indicating that the formation of Mn^{2+} species is significant. The observed oxygen composition is 21.3%. The stoichiometrically estimated percentage for these oxygens is about 17% in total, indicating the surface is also oxygen-enriched.

However, studies on the 450 h catalyst reveals that 97% of the tungsten species observed on the fresh catalyst by XPS disappeared, and the W L_{III}-edge was not detectable
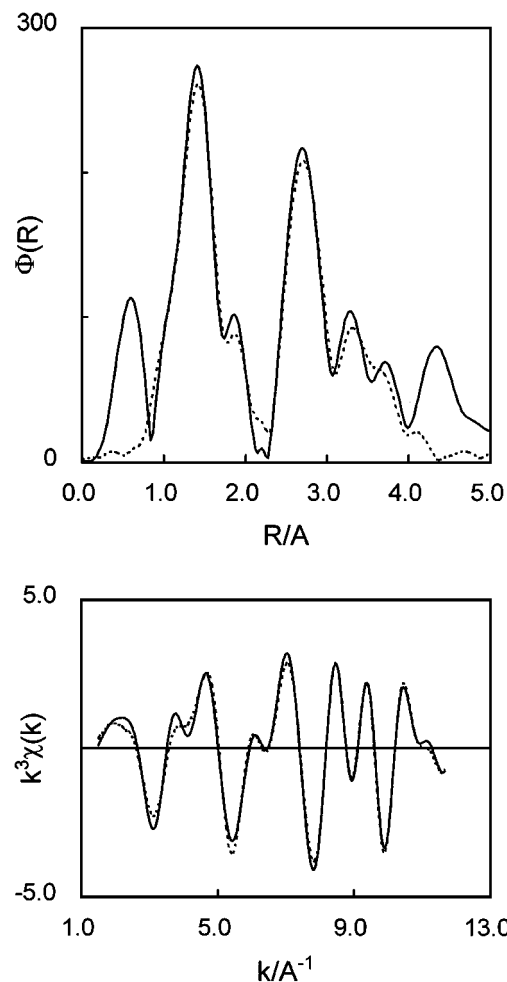

FIG. 7. Amplitude analysis of Mn K-edge EXAFS oscillation: (A) filtered from the manganese contribution in the Fourier transform of Mn_2O_3; (B) filtered from the peak labeled Mn in Fig. 4; and (C) filtered from the peaks labeled W in Fig. 4.

completely coordinatively saturated by 6 oxygens. (ii) each manganese in addition has about 2 manganese neighbors at 3.14 Å, which is almost identical to the Mn–Mn distance (3.13 Å) in the reference oxide Mn_2O_3. (iii) each manganese has about 3 tungsten neighbors at 3.6, and 4.2 Å, respectively. In a geometrical consideration, the former Mn–W distance of 3.6 Å can be achieved by sharing the same oxygen neighbor, i.e., by the formation of Mn–O–W bonds, but the latter seems too long to fit the geometry.

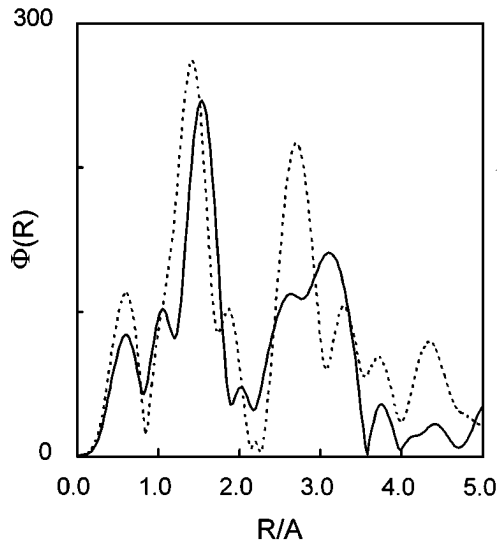**FIG. 8.** The best fits (dashed lines) to the Mn K-edge EXAFS and the Fourier transform of the fresh catalyst.

FIG. 9. Comparison of the Mn K-edge EXAFS-derived Fourier transform of the used catalyst (solid line) with that of the fresh sample.

major features labeled A, B, and C in the edge region. The pre-edge peak A reflects the transitions of 1s to empty 3d orbitals. It is dipole forbidden (but quadrupole allowed) for regular octahedral site-symmetry, a very weak peak is thus generally observed for MnO_2 and Mn_2O_3. However, 1s → 3d transition is dipole-allowed for a tetrahedral symmetry. In this case, the more empty the 3d orbitals, the more intense the pre-edge peak is expected. In comparison with the half-filled Fe^{3+} in iron-containing silicate glass (40), the Mn^{7+} in $KMnO_4$ is a very special example. Both are in tetrahedral coordination, however, the relative intensity of the pre-edge peak is only 0.08 for the half-filled Fe^{3+} but is 0.69 for the fully empty Mn^{7+}. The rapidly growing edge is a sensitive indicator of the ionization threshold. Since the feature C is originated from the transitions of 1s to 4p final states, the possible transitions from 1s to the orbitals below 4p are expected to be observed at the edge. For example, a shoulder added to the onset of the raising edge is frequently but empirically assigned to 1s → $4p_z$ transitions for 3d-metal complexes (35–38).
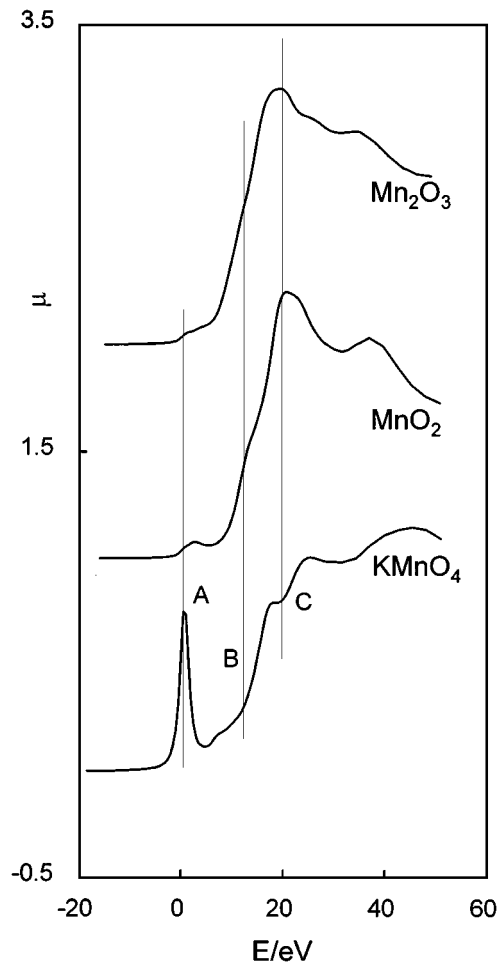
in the XAFS measurement. Mn K-edge EXAFS-derived Fourier transform of the 450 h catalyst is shown in Fig. 9. In comparison with that of the fresh catalyst, the most intense peak originating from the nearest oxygens shifts to higher r-space significantly, suggesting a lengthened Mn–O bond. Correspondingly, the area of the peak decreases, indicating a lower coordination number for the shell. Above the Mn–O shell, a fairly intense, broad peak is observed in the range of 2.2–4.0 Å. The peak containing broad shoulders significantly deviates from Gaussian distribution, implying a complicated environment for the manganese ions. Thus, only the most intense peak in the transform is Fourier-filtered and fitted in k-space. The structural parameters therefrom is summarized in Table 4. 4.3 nearest oxygens at a longer distance of 2.09 Å are obtained. Meanwhile, a predominant Mn $2p_{3/2}$ peak at 641.9 eV with a Mn^{2+} shake-up shoulder is well observed by XPS, as shown in Fig. 6. The peak consists of two contributions, one is at 641.4 eV (Mn^{3+}) while the other is at 641.9 eV. According to its correlation to the Mn^{2+} shake-up shoulder at 646.7 eV, the binding energy of 641.7–641.9 eV is attributed to Mn^{2+} by referring to the Mn^{2+} in $MnSO_4$. The relative ratio of Mn^{3+}/Mn^{2+} on the 450 h catalyst determined by the best fit is about 1 : 3.4.

In order to better understand what was happened for the manganese species on the surface, Mn K-edge XANES spectra were recorded. The features in the Mn K-edge XANES region have not been clearly interpreted in the literature (25, 26). However, extensive studies on the XANES of 3d-metal complexes have considerably improved our understanding (27–40). It can be seen, for example, from the Mn K-edge XANES of the reference compounds MnO_2, Mn_2O_3, and $KMnO_4$ shown in Fig. 10 that there are three

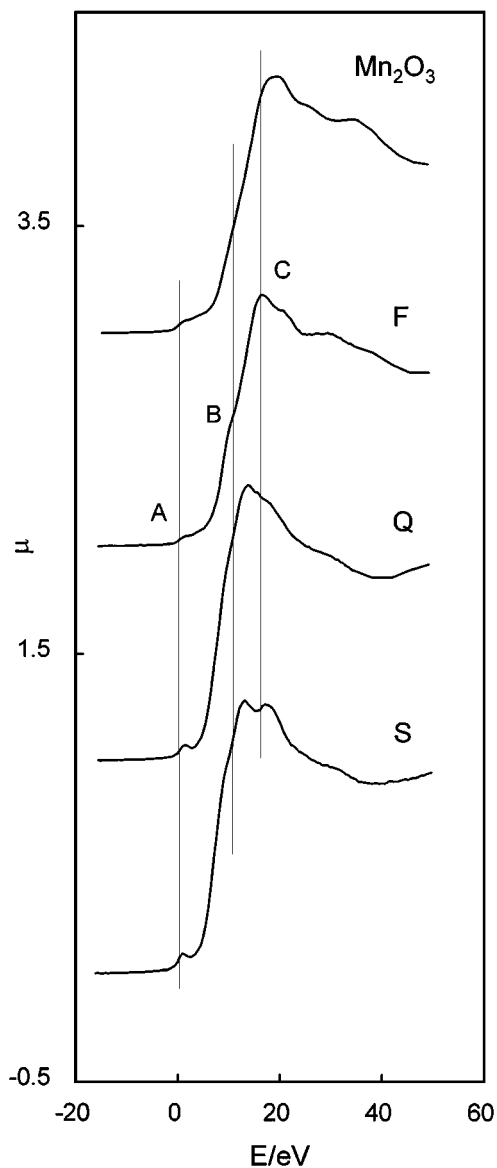**FIG. 10.** The manganese K-edge XANES spectra of the reference compounds.

FIG. 11. The Mn K-edge XANES spectra for the fresh catalyst (F), the quenched catalyst after a 100 h run (Q) and the used catalyst (S).

The Mn K-edge XANES spectra of the fresh catalyst Mn/Na$_2$WO$_4$/SiO$_2$ (F), the 100 h catalyst (Q), and the 450 h catalyst (S) are compared in Fig. 11. The XANES features of the supported oxides are generally somewhat complex probably because of mixing of various symmetries. It can be seen however that the features of F are closely similar to those of Mn$_2$O$_3$ but not MnO$_2$, indicating the formation of Mn$_2$O$_3$ phase on the surface. It has been found from F to Q, and to S that (i) the intensity of the pre-edge feature is consistently increased from 0.04, 0.06 to 0.09, indicating the gradual formation of tetrahedral sites. Noticing that the Mn^{2+} determined by XPS has the same d-orbitals as that of Fe^{3+}; (ii) the shoulder at the onset of the edge, feature B, which is not clear enough in the XANES of Mn$_2$O$_3$, is well

resolvable in that of the fresh catalyst and more intense in that of the used catalysts, indicating the consistent increase of empty axial ligand sites for the originally coordinatively saturated octahedral manganese cores; (iii) as the Mn–O bond length increases from F (2.00 Å) to S (2.09 Å), the energy difference between the pre-edge feature, peak A, and the 1s-4p feature, peak C, decreases significantly. It is 20.2 eV for F, 18.2 eV for Q, but only 17.2 eV for S. Similar phenomenon has been interpreted by Bianconi (40).

5. Understanding of the Surface

For the formation of an electronically neutral surface, WO$_4$ group does not need to connect with the silica surface very tightly, for example, in a triply bridged mode (4). In this sense, the study on silica-supported Re$_2$O$_7$ is very informative (41). The reaction of Re$_2$O$_7$ with the siloxane bridges leads to the formation of surface perrhenates. For our system, two tungsten ions (W^{6+}) share one bridging oxygen and each binds to silica surface via a single oxygen is enough to maintain their electro-neutrality. Such a group of tungsten species is easier to be enriched and to move on the surface, and finally completely disappeared from the surface under fluidized bed conditions. Infrared analysis seems in good agreement with this estimation. A broad band at 2020.7 cm^{-1} is observed for the fresh catalyst, but is completely absent for the 450 h catalyst. In accordance with the XPS results that 97% tungsten species are not observable on the 450 h catalyst, this broad band is thought to correspond to the WO$_4$ groups, which may show the bands similar to the Re$_2$O$_7$/SiO$_2$. The bands observed for Re$_2$O$_7$/SiO$_2$ are 1989, and 1850 cm^{-1}, respectively, while the calculated value is 2030 cm^{-1} (41).

However, when the formation of a neutral surface is considered, the manganese ions have a different story. As indicated by the best fits (Table 4), each of the manganese ions on the fresh catalyst is coordinatively saturated by 6 oxygen neighbors, that is, a single Mn^{3+} cannot exist on the surface unless it is contained in a group of manganese ions or in a system of manganese-tungsten mixture. In both cases, the silica-support must be closely involved since the surface is not enriched in Mn as determined by XPS. For example, when the geometric understanding of Fe$_3(\mu_3$-CO)CO$_6$ (23) is applied here, it can be estimated that three Mn^{3+} ions could form a cluster having a formula of either Mn$_3(\mu_2$-O)$_3$O$_3$ or Mn$_3(\mu_3$-O)O$_6$. If each of the manganese were located in a triply bridged site on surface, it would have a 6-coordinated, octahedral site-symmetry. Even so, however, they would be stoichiometrically in the form of Mn$_3$O$_6$ or Mn$_3$O$_7$ with extremely high electro-negativity (−3 or −5), participation of the sodium cations and/or the formation of Mn$_{20}$O$_{30}$ ensembles (24) must still be extremely necessary. It is the reason why a significant amount of manganese ions (about 2/5) has to be retained in a small crystalline form although their loading (<2 wt%) is not high,

and why the surface of the fresh catalyst is not possible to be enriched in Mn. The other 3/5 manganese ions kept in an amorphous state have to disperse themselves into WO_4 groups and/or silica substrate by the formation of W−O−Mn bonds or Mn−O−Si bonds. The former is demonstrated by 2 tungsten neighbors at 3.6 Å from the Mn K-edge EXAFS results, the latter, however, unfortunately, is not technically available by EXAFS analysis since the Mn−Si distance would be expected to have a similar value of 3.6 Å.

The amorphous feature of the $Mn/Na_2WO_4/SiO_2$ catalyst has been well recognized by the characterization results. Structural studies on crystalline Mn_2O_3 have suggested that the manganese ions tend to maintain a 4-coordinated, square planer geometry (D_{4h}) by making two axial oxygen sites empty (42), implying that Mn_2O_3 will be a good oxygen releaser. On the other hand, studies on Na_2WO_4/SiO_2, Na_2WO_4/CeO_2, and $NaMnO_4/SiO_2$ seem to suggest that tetrahedral transition metal sites (T_d) are necessary for the activation of methane. Thus, an active T_d site accompanied with a good oxygen-releaser must be an effective catalytic ensemble for the oxidative coupling of methane. For the case of this study, we have

$$T_d\text{-}W^{6+} \leftrightarrow D_{4h}\text{-}Mn^{3+} \leftrightarrow O_h\text{-}Mn^{3+}$$

Two tentative structural models involving the possible formation of active oxygen species are considered for the surface ensembles, as shown in Fig. 12.
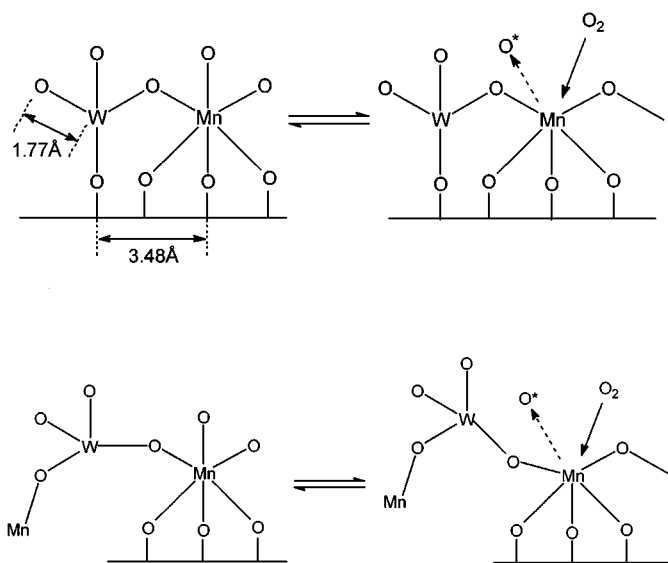

FIG. 12. Two tentative models involving the possible formation of active oxygen species (O^*). Notice: Unlike that of WO_4 groups, mononuclear MnO_6 species CANNOT exist alone on surface as stated in the discussion. The Mn center shown in the scheme must be stoichiometrically bounded into an ensemble of either Mn_2O_3 (for example, $Fe_{20}O_{30}/Al_2O_3$, Ref. (24)) and/or WO_4−Mn_2O_3−SiO_2 complexes. The situation, however, is not shown for the sake of clarity.

IV. CONCLUSION

In conclusion, this work encourages us to propose that the combination of two cationic centers with different oxidation states and site-symmetries from each other would be expected without exception to present a certain catalytic activity for the oxidative coupling of methane. In the case of the manganese-tungsten catalyst, for example, the tungsten in a T_d-center is responsible for the activation of methane while the manganese in an O_h-center is responsible mainly for the transformation and transportation of oxygens. The combination of the two centers can therefore transfer electrons and oxygens simultaneously. It has to state in this view that it is the nearest oxygens but not the lattice oxygens which are to be responsible for the high performance of $Mn/Na_2WO_4/SiO_2$ in the reaction, i.e., it is the amorphous feature of the catalyst to effectively activate the lattice oxygens to the nearest oxygens before the catalysis occurs. This conclusion is fully supported by the results obtained from the used catalysts. As the WO_4 groups gradually disappear from the surface, tetrahedrally coordinated Mn^{2+} sites are formed on the surface probably through the formation of square-planer Mn^{3+}/Mn^{2+} sites. Thus, $T_d\text{-}Mn^{2+} \leftrightarrow D_{4h}\text{-}Mn^{2+}/Mn^{3+} \leftrightarrow O_h\text{-}Mn^{3+}$ begins to perform the catalysis continuously. The coordination number of the nearest oxygens observed is thus significantly decreased to only about 4 after a 450 h run. The reaction data revealed that the amount of CO_2 in the products decreased significantly for the last 200 h. On the other hand, the amount of CO increased, and finally reached the initial level of CO_2 (9). These results suggest that the manganese species as a good oxygen-releaser is not as good as an oxygen-catcher. It is therefore hopeful from this study that a more effective and stable catalyst than the $Mn/Na_2WO_4/SiO_2$ will be available in the future if the T_d-center is more tightly bound to the surface and if the O_h-center is a much better oxygen-carrier good at catching as well as releasing oxygens simultaneously.

In addition, regarding to the disappearance of the surface tungsten species, we tend to note here that the operation in a fluidized bed mode and the superheated steam environment in the reactor in deed significantly aggravate the loss of the tungsten species since the tungstens are weakly bound to and are enriched on the surface.

REFERENCES

1. Fang, X., Li, S., Lin, J., Gu, J., and Yang, D., *J. Mol. Catal. (China)* **6**, 225 (1992).
2. Fang, X., Li, S., Lin, J., and Zhu, Y., *J. Mol. Catal. (China)* **6**, 427 (1992).

3. Jiang, Z., Yu, C., Fang, X., Li, S., and Wang, H.-L., *J. Phys. Chem.* **97**, 12870 (1993).

4. Wu, J., Li, S., Niu, J.-Z., and Fang, X., *Appl. Catal.* **A124**, 9 (1995).

5. Wu, J., and Li, S., *J. Phys. Chem.* **99**, 4566 (1995).

6. Lunsford, J. H., *Angew. Chem. Int. Ed. Engl.* **34**, 970 (1995).

7. Yu, Z., Yang, X., Lunsford, J. H., and Rosynek, M. P., *J. Catal.* **154**, 163 (1995).

8. Wang, D., Rosynek, M. P., and Lunsford, J. H., *J. Catal.* **155**, 390 (1995).

9. Wang X., and Li, S., *Shiyou Huagong,* **26**(6), 381 (1997).

10. Shluger, A. L., Gale, J. D., and Catlow, C. R. A., *J. Phys. Chem.* **96**, 389 (1992).

11. Yang, T.-L., Feng, L.-P., and Shen, S.-K., *J. Catal.* **145**, 384 (1994).

12. Bukhtiyarov, V. I., Boronin, A. I., and Savchenko, V. I., *J. Catal.* **150**, 262 (1994).

13. Bukhtiyarov, V. I., Boronin, A. I., Prosvirin, I. P., and Savchenko, V. I., *J. Catal.* **150**, 268 (1994).

14. Islam, M. S., Ilett, D. J., and Parker, S. C., *J. Phys. Chem.* **99**, 9637 (1994).

15. Xu, M., Ballinger, T. H., and Lunsford, J. H., *J. Phys. Chem.* **99**, 14494 (1995).

16. Au, C. T., He, H., Lai, S. Y., and Ng, C. F., *J. Catal.* **163**, 399 (1996).

17. Rehr, J. J., Mustre de Leon, J., Zabinsky, S. I., and Albers, R. C., *J. Am. Chem. Soc.* **113**, 5135 (1991).

18. Lytle, F. W., Sayers, D. E., and Stern, E. A., *Physica B* **158**, 701 (1989).

19. Cox, A. D., *in* "EXAFS for Inorganic Systems," DL/SCI/R17, Daresbury, 1981.

20. Horsley, J. A., Wachs, I. E., Brown, J. M., and Hardcastle, F. D., *J. Phys. Chem.* **91**, 4014 (1987).

21. Cotton, F. A., and Wilkinson, G., "Advanced Inorganic Chemistry," 4th ed., p. 850. Wiley, New York, 1980.

22. Kou, Y., Wang, H.-L., Te, M., Tanaka, T., and Nomura, M., *J. Catal.* **141**, 660 (1993).

23. Kou, Y., Suo, Z.-H., and Wang, H.-L., *J. Catal.* **149**, 247 (1994).

24. Kou, Y., Wang, H.-L., Niu, J.-Z., and Ji, W.-J., *J. Phys. Chem.* **100**, 2330 (1996).

25. Peng, G., deGroot, F. M. F., Hämäläineu, K., Moore, J. A., Wang, X., Grush, M. M., Hastings, J. B., Siddons, D. P., Armstrong, W. H., Mullins, O. C., and Cramer, S. P., *J. Am. Chem. Soc.* **116**, 2914 (1994).

26. Grush, M. M., Christon, G., Hämäläineu, K., and Cramer, S. P., *J. Am. Chem. Soc.* **117**, 5895 (1995).

27. Shulman, R. G., Eisenberger, P., Blumberg, W. E., and Stombaugh, N. A., *Proc. Natl. Acad. Sci.* **72**, 4003 (1975).

28. Smith, T. A., Penner-Hahn, J. E., Berding, M. A., Doniach, S., and Hodgson, K. O., *J. Am. Chem. Soc.* **107**, 5945 (1985).

29. Eidsness, M. K., Sullivan, R. J., Schwartz, J. R., Hartzell, P. L., Wolfe, R. S., Flank, A. M., Cramer, S. P., and Scott, R. A., *J. Am. Chem. Soc.* **108**, 3120 (1986).

30. Blackburn, N. J., Strange, R. W., MaFadden, L. M., and Hasnain, S. S., *J. Am. Chem. Soc.* **109**, 7162 (1987).

31. Sano, M., *Inorg. Chem.* **27**, 4249 (1988).

32. Clark, K., Penner-Hahn, J. E., Whittaker, M. M., and Whittaker, J. W., *J. Am. Chem. Soc.* **112**, 6433 (1990).

33. Sagi, L., Wirt, M. D., Chen, E., Frisbie, S. M., and Chance, M. R., *J. Am. Chem. Soc.* **112**, 8639 (1990).

34. Furenlid, L. R., Renner, M. W., Smith, K. M., and Fajer, J., *J. Am. Chem. Soc.* **112**, 8987 (1990).

35. Furenlid, L. R., Renner, M. W., Szalda, D. J., and Fujita, E., *J. Am. Chem. Soc.* **113**, 883 (1991).

36. Whitehead, J. P., Colpas, G. J., Bagyinka, C., and Maroney, M. J., *J. Am. Chem. Soc.* **113**, 6288 (1991).

37. Nelson, M. J., Jin, H., Turner, I. M., Jr., Grove, G., Scarrow, R. C., Brennan, B. A., and Que, L., Jr., *J. Am. Chem. Soc.* **113**, 7072 (1991).

38. Kim, S., Bae, I. T., Sandifer, M., Ross, P. N., Car, R., Woicik, J., Antonio, M. R., and Scherson, D. A., *J. Am. Chem. Soc.* **113**, 9063 (1991).

39. Bianconi, A., Garcia, J., and Benfatto, M., Topics in Current Chemistry, **145**, 29 (1988).

40. Bianconi, A., Fritsch, E., Calas, G., and Petiau, J., *Phys. Rev.* **B32**, 4292 (1985).

41. Scott, S. L., and Basset, J.-M., *J. Am. Chem. Soc.* **116**, 12069 (1994).

42. Christ, C. L., "Descriptive Crystal Chemistry." Wiley, New York, 1989.